JOURNAL OF MATERIALS SCIENCE 15 (1980) 387–404

Rayleigh wave interaction with, and the extension of, microcracks

M. V. SWAIN*
Saint-Gobain Industries, Service Central de Recherche, Aubervilliers, France
J. T. HAGAN
Cavendish Laboratory, Madingley Road, Cambridge, UK

Intense Rayleigh waves produced by the impact of high-velocity liquid jets on brittle solids were arranged to interact with well-defined surface flaws of dimensions 50 to 200 μm. The extent of crack growth was monitored as a function of distance from the impact site. It was found that considerable crack growth as well as crack branching occurred for cracks parallel to the incident wavefront and little or no growth for orthogonal cracks. The form of the surface wave was monitored using piezoelectric crystals attached to the surface. The results are discussed in terms of recent fracture mechanics analysis of stress-wave interaction with cracks. The significance of this study to strength degradation of brittle bodies subjected to rain-drop impact is pointed out.

1. Introduction

The response of brittle solids to transient stress pulses resulting from the impact of high-velocity solids or liquid drops is of considerable interest because of its significance to strength degradation and erosion. As the majority of flaws in brittle solids lie in the surface of the material, the interactions of these flaws with transient surface waves produced by such impacts can play a major role in strength degradation. These problems may arise in such practical situations as cavitation damage on turbines and the damage of brittle materials (e.g. forward facing radomes on aircraft) impacted by rain drops and small deformable solid particles such as plastics.

There have recently been a number of papers both theoretical and experimental which have considered the problem of a tensile stress wave interacting with a crack. Theoretical treatments of this problem have been carried out by Sih *et al.* [1], Thau and Lu [2], and also by Freund [3]. Freund has considered the case of a semi-infinite crack whereas Sih *et al.* and Thau and Lu considered a crack of finite size.

The interesting feature to emerge from the latter studies is that the stress intensity factor is a function of time, the maximum value exceeds the quasi-static value by approximately 25%. This prediction has been confirmed in principle by the recent work of Kalthoff and Shockey [4] who observed the growth of internal penny-shaped cracks in polycarbonate subjected to very short duration tensile stress pulses. Also Vardar and Finnie [5] have studied the fracture produced in brittle rocks subjected to short, intense, tensile pulses produced by a high-energy electron beam.

The particular case of a Rayleigh or surface wave incident upon a crack in the surface of a semi-infinite solid has received only cursory examination. Freund [6] has considered the case of a Rayleigh wave travelling along the crack interface and its interaction with the crack tip. However, photo-elastic observations of Rayleigh waves interacting with narrow slots of various lengths have been carried out by Rhinehardt and Dally [7]. These authors noted that, as well as reflection of the surface wave from the slots, a surface wave was propagated down the face of the slot, also

* Present address: CSIRO, Division of Materials Science, Engineering Ceramics, and Refractories Laboratory, 506 Lorimer Street, Fisherman's Bend, Victoria, Australia, 3207.

0022–2461/80/020387–18$03.80/0

some mode conversion occurred. Similar observations have been made by Bond [8] in a study of surface waves interacting with a right-angled corner using finite difference techniques. Rhinehardt and Dally [7] also observed that the stress field in the vicinity of the tip of the slot was a function of the ratio of the slot depth to wavelength of the surface wave. For flaws approaching a wavelength and more in depth, the principle tensile direction was almost parallel to the free surface of the plate, whereas for small flaws it was normal to the surface. Previous studies by Bowden and Field [9] and Field [10] have shown that surface waves are capable of initiating surface flaws as they traverse the surface at distances well away from the impact site. They also observed in thin plates concentric zones of enhanced microcracking resulting from reinforcement of the surface wave with reflections of compressional waves from the rear surface of the plate.

More recently, Rickerby [11] has shown that the impact of high-velocity water jets, which produce short duration surface waves, onto glass discs results in a decrease of strength with increasing velocity. The observed decrease in strength was very similar to that reported by Evans [12] for strength reduction resulting from Hertzian cone crack formation. However, unlike low-velocity solid particle impact, the contact time and contact pressures involved in water droplet or jet impact are still poorly understood. A recent review of water droplet impact and of the pressures developed beneath the impact site has been given by Adler [13]. A theoretical analysis of the stresses produced by a liquid drop on a rigid elastic half-space has been carried out by Blowers [14]. This treatment considers a uniform pressure over the area of contact and the development of the stresses in the half space, it enables the magnitude of the stresses at any position or time during loading to be determined. However, this analysis does not incorporate a flow criteria for the fluid and subsequent development of the stress field. The solutions generated by Blower's analysis have been used by Evans and Wilshaw [15] and by Adler [13] to explain and predict the regions of crack growth resulting from high-velocity impact by water drops and plastic spheres.

The stresses and displacements produced by a point, rapidly loading and unloading the surface of an elastic half-space, were first examined by Lamb [16]. Subsequent theoretical treatments by Peckeris [17] and by Miller and Pursey [18] verified Lamb's conclusion that the intensity of the surface wave falls off as $R^{-1/2}$, where R is the radial distance from the source. Mooney [19], in a recent review of surface waves produced by point contact, has generalized the solutions [20] to finite contact times for both normal and tangential loading. A limited number of experimental observations have confirmed the theoretical treatments of Lamb and subsequent workers. The essential prediction of the decrease in the magnitude of the stress with distance was verified by Goodier *et al.* [21]. The form of the stress waves produced by a sudden unloading event [22], also verifies very well the theoretical productions. Tsai and Kolsky [23] have monitored the stress waves produced by a ball dropping onto an elastic half-space; these are somewhat similar to those predicted by Mooney [20].

In this paper we present some observations of the extent of crack growth produced by high-velocity liquid jets. Cracks of well-defined orientation and direction have been introduced into the surface of a large block of glass and the extension of these cracks during the stress-wave loading has been measured. The form of the stress waves has been monitored using piezoelectric crystals for both jet and ball impact and very good agreement with the predictions of Mooney [19] is found.

2. Theoretical considerations

2.1. Impact pressure and time of contact

A liquid drop or jet on impact initially behaves compressibly until release waves from the edge reach the centre of contact. Thereafter, flow occurs and the pressure is given by the hydrodynamic "stagnation" pressure, p_0

$$p_0 = \tfrac{1}{2}\rho V^2 \tag{1a}$$

where ρ is the density of the liquid and V is the velocity of the jet or drop. The initial impact pressure, or "water hammer" pressure is given by

$$p_0 = \rho C V \tag{1b}$$

where C is the velocity of compressive waves in the liquid. A more precise expression for the initial impact pressure, which takes into account the compressibility of the solid under impact as well as that of the impinging liquid, is given by

$$p_0 = \frac{\rho C V}{1 + (\rho C/\rho_s C_s)} \tag{1c}$$

where ρ_s and C_s are the density and velocity of compressive waves in the solid. The distribution of normal pressure beneath the area of contact has been suggested, as being similar to that beneath a sphere [30], and more recently as that beneath a cylinder [46], in contact with a flat surface. However, the predictions of these two pressure distributions are basically different with the former, the pressure decreasing to zero at the edge whereas the latter predicts a maximum at this position. Johnson and Vickers [46] present experimental evidence, for low-velocity jets, closer to the stress distribution beneath a cylinder in contact with a flat surface. More recently, an experimental and theoretical analysis of the break-up of high-velocity jets by Field and Lesser [47] suggests that cavitation occurs near the edge of the jet. This phenomena would have the effect of locally reducing the density of the jet close to the edge and hence the normal impact pressure in this region.

The duration of the "water hammer" pressure is determined by the time for release waves to travel across the radius of contact and flow to occur. In the case of a cylindrical jet of water, Bowden and Field [9] suggested the time of contact is given by

$$T \simeq r/C \tag{2}$$

where r is the radius of the jet at contact.

2.2. Stress waves produced

The impact of a solid or incompressible liquid onto an elastic half-space produces dilational, shear and Rayleigh surface waves which radiate from the impact site. The analytical description of the surface waves was first carried out by Lamb [16]. Subsequent work by a number of authors (see Mooney [19] for a recent review) has extended Lamb's analysis to consider the effect of finite contact area, finite loading time, as well as tangential loading. For the case of finite contact time and area of contact the behaviour close to the contact region is very complicated but the far field solutions are very similar to those proposed by Lamb [16]. The major difference between a step function application of load and a Hertzian impact onto an elastic half-space is that the latter results in a rounding off and reduction in intensity of the peaks as well as an increase in the temporal duration of the surface wave.

The shear and dilational waves produced by the impact are least at the surface where their intensities fall off as R^{-2}, whereas into the bulk they fall off as R^{-1}. The intensity of the surface wave falls off as $R^{-1/2}$ and consequently will be of greatest significance at distances large compared with the contact diameter. Miller and Pursey [18] have calculated the energy radiated by an impact onto an elastic half-space and find that 67% of the dissipated energy is in the Rayleigh wave. Mooney [20] has found that the intensity of surface waves was proportional to the pulse length T and initial amplitude of the source pulse D and may be expressed as

$$I \propto DR^{-1/2}T^{-3/2} \tag{3}$$

for detectors that measure horizontal strain. The variation of the radial and vertical components of stress with depth for a surface wave are shown in Fig. 1. It is apparent that the radial component changes sign at a depth of approximately $\frac{1}{5}$ of the wavelength of the surface stress pulse.

The form of the radial stress produced by the impact of a ball has been calculated by Tsai and Kolsky [23]. Mooney [20] has calculated the radial strains for a generalized loading which is similar to that of a ball impact. In the solutions by both authors there are a number of simplifying approximations. Tsai and Kolsky allow for a finite contact area and time of duration but keep the contact diameter constant throughout the contact. Mooney on the other hand only considers an ideal point contact but allows both an impulsive loading as well as a more realistic loading history. The forms of the radial strain as predicted by Tsai and Kolsky, and by Mooney are shown in Fig. 2. The solutions presented in Fig. 2 are probably

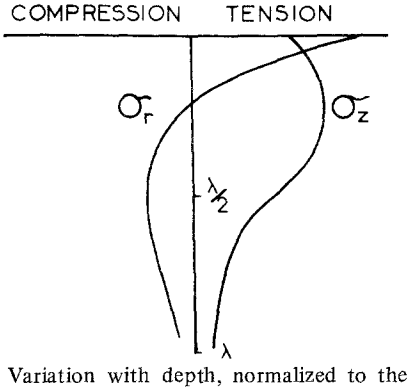

Figure 1 Variation with depth, normalized to the wavelength λ, of the radial, σ_r, and vertical σ_z, components of stress associated with a Rayleigh wave ($\nu = 0.25$). After Graff [27].

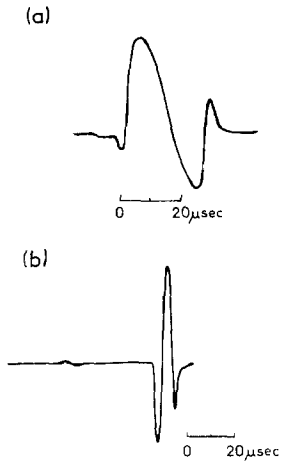

Figure 2 Predicted radial strain of a Rayleigh wave produced by: (a) the impact of a 6.35 mm diameter steel sphere onto soda-lime glass, 2 cm from the detector with a duration of contact 25 μsec, according to Tsai and Kolsky [23], (b) for a sphere-like impact of duration 10 μsec onto granite 30 cm from the detector, according to Mooney [20].

valid for the far field stress fields, that is at distances at least 2 or 3 contact diameters away from the axis of contact. In comparison, Blowers [14] has computed the development of the stress field resulting from the impact of an incompressible fluid onto an elastic half-space with uniform pressure over the expanding area of contact. It is possible from this analysis to determine the stress at any position in the half-space as a function of elapsed time after contact. Adler [13] has recently used this analysis to compute the stress fields produced by a rain drop in a number of materials. A typical example of the predicted radial stress produced by the impact of a 1.8 mm diameter water drop onto a glass block at 220 m sec^{-1} is shown in Fig. 3. Unfortunately, it was not possible

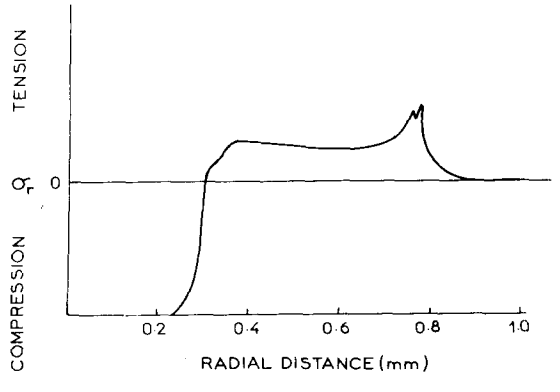

Figure 3 The radial stress predicted by Blowers analysis for a 1.8 mm droplet impacting soda-lime glass at 220 m sec^{-1} 0.237 μsec after contact, according to Adler [13].

to generate the stresses at the surface but reasonable values are obtained 10 μm below the surface, and also it is not possible to follow the stress wave behaviour after flow has occurred. In the present study more emphasis is placed upon the far field solutions because they have been measured and because it is at distances removed from the contact site that crack extension has been studied.

2.3. Dynamic fracture mechanics

The problem of a crack subjected to a plane dilational wave has been treated by a number of authors [1–3, 24]. The essential feature to emerge from these studies is that the stress intensity factor is initially a function of time. The crack diffracts the stress wave and for a finite crack, the maximum stress intensity occurs in the time for a Rayleigh wave to travel from one crack tip to the other. Thereafter, provided the crack remains stationary, the stress intensity factor exhibits damped oscillatory behaviour about the quasi-static value. For a semi-infinite crack the dynamic stress intensity factor may be written [5],

$$K_d(t, 0) \simeq 1.3\sigma_0\sqrt{\left(\frac{\pi C_r t}{2}\right)}. \quad (4)$$

For non-step-function stress-wave loadings, the stress intensity factor may be determined by a method suggested by Freund [6]. He considers the case of a large number of infinitesimally small step-function loadings and finds that in the limit, the stress intensity factor is:

$$K_d(t,0) = 1.3\sqrt{\left(\frac{\pi C_r}{2}\right)}\int_0^t \sigma(s)(t-s)^{1/2}\,ds. \quad (5)$$

By way of comparison with a square wave, the stress intensity factors for a triangular wave of the same intensity, as shown in Fig. 4a, are given by:

$$K_d(t,0) = 2.12\sigma_0\sqrt{(C_r t)}\left[\left(\frac{t}{t_0}\right)^{3/2} - H(t-t_0/2)\left\{2\left(\frac{t}{t_0}-\frac{1}{2}\right)^{3/2}\right\}\right] \quad (6)$$

where $H(t-t_0/2)$ is a Heaviside step function.

Because the stress intensity factor for stress-wave loading of a crack is a function of time, there will be some delay before the threshold K_{IC} value is achieved. This is shown in Fig. 4b and it varies considerably for each loading pulse. For the case of a square pulse, it is easily shown that the incubation time, τ, is given by:

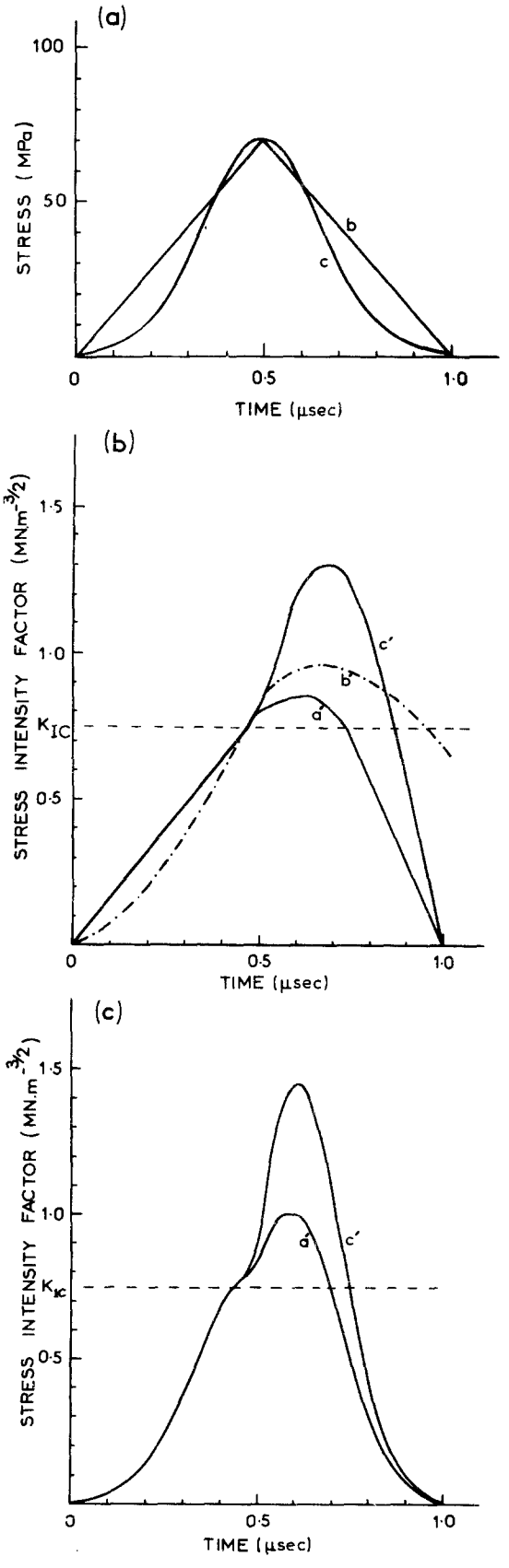

Figure 4 (a) Stress pulses for which the stress intensity factors have been determined. Variation of the stress intensity factor with time for, (b) triangular, (c) error function. In each figure a' is as predicted by Equation 13, b' is the dynamic stress intensity factor, and c' the quasi-static value.

$$\tau = \frac{1.18K_{IC}^2(1-\nu^2)}{\sigma_0^2 \pi C_r}. \tag{7}$$

This expression is similar to one given by Freund [6], who also found that the incubation time was a sensitive function of the angle of incidence between the flaw and the stress wave. If the crack tip stress intensity factor exceeds K_{IC} the crack will extend. Any determination of the subsequent stress intensity factor at the crack tip must consider the velocity of the crack. The dynamic stress intensity factor for a crack with velocity, V, is given by:

$$K_d(t, V) = k(V)K_d(t, 0) \tag{8}$$

where $k(V)$ is a modifying factor which varies with velocity. Broberg [25] was first to show that $k(0) = 1$, and $k(C_r) = 0$. A simpler approach is to consider the fracture toughness variation with velocity, which may be written

$$\frac{G_d(t, V)}{G_d(t, 0)} = g(V) \simeq \left(1 - \frac{V}{C_r}\right) \tag{9}$$

where

$$G_d(t, V) = \frac{K_{IC}^2}{E}(1-\nu^2) \quad \text{(plane strain)}.$$

It is now possible to determine for a given stress wave loading pulse the crack velocity as a function of time. For the case of a material with its fracture toughness independent of velocity we have

$$V = C_r\left(1 - \frac{K_{IC}^2}{K_d^2}\right). \tag{10}$$

Evans [26] has recently used such an approach to predict the extension of cracks subjected to square-wave pulses. A more generalized expression which allows the fracture toughness to vary with velocity has been considered by Bergkvist [33] with particular reference to crack growth in PMMA.

Knowing the variation of velocity of the cracks with time during the course of the stress wave loading it is possible to determine the growth of these cracks, that is

$$\Delta C = \int_{t_1}^{t_2} V \, dt \tag{11}$$

where the limits, t_1 and t_2 are determined when K_d equals K_{IC}. For the case of a triangular stress pulse we have from Equations 6, 10 and 11:

$$\Delta C = C_r \left\{ [t]_{t_1}^{t_2} + \left[\frac{2K_{IC}^2}{3\sigma_0^2 \pi C_r} \left(\frac{t_0}{t} \right)^2 \right]_{t_1}^{t_0/2} - \left[\frac{6K_{IC}^2}{\sigma_0^2 C_r \pi} \left\{ \left(\frac{t}{t_0 - 3t} \right) - \log \left(3 - \frac{t}{t_0} \right) \right\} \right]_{t_0/2}^{t_2} \right\}. \quad (12)$$

Somewhat similar expressions may be derived for sinusoidal or square-pulse loading.

An alternative method of determing the stress intensity factor of a growing crack has been suggested by Eshelby [38]. This analysis was developed for mode III cracks but might be expected to give reasonable estimates for mode I crack growth. Eshelby's approach acknowledges the initial size of the crack and that after crack initiation the crack does not know its own length. The stress intensity factor is given by:

$$K = m\sigma(\pi a)^{1/2} \left(1 - \frac{V}{C_r} \right)^{1/2} U \quad (13)$$

where a is the initial crack length, and U is given by the following series

$$U = \left[1 + \frac{3}{8} \left(\frac{c-a}{a} \right) - \frac{15}{256} \left(\frac{c-a}{a} \right)^2 + \ldots \right]$$

or may be expressed in terms of elliptical integrals.

The incubation time for the initiation of a flaw is now given by the quasi-static conditions and depends only upon the time variation of stress. This expression is far more applicable to small flaws where the transit time of a Rayleigh pulse from one crack tip to the other is very much less than the duration of the pulse, that is $2a \ll C_r t_0$. However, once the crack has extended a few times its initial length self-similar or quasi-steady solutions for the stress intensity factor are more appropriate (Broberg [25]). The stress intensity factor is then given by, again for mode III cracks

$$K = m\sigma(\pi c)^{1/2} k/E$$

where $k = (1 - V^2/C_r^2)$ and E is a complete elliptical integral of the second kind with modulus k. Rose [43] has considered these two approaches as well as a quasi-static approach to predict the initial motion of a Griffith crack in a uniform stress field. The extension of these concepts to a rapidly varying stress field will only be expected to give approximate solutions.

Although the above approach is far more satisfactory for small flaws in time varying stress fields it is difficult to predetermine the stress intensity factor after crack initiation and hence predict crack growth. This is because the stress intensity factor is a function of crack length and velocity of the crack.

An approximate method which enables an estimate of crack growth is to compute the stress intensity factor for small increments of time after crack initiation and assume constant velocity during this time increment. This has been done for two particular stress pulses: triangular and error function, Fig. 4a. The resulting stress intensity factors for a maximum stress of 70 MPa normally incident on a flaw of 50 μm in soda-lime glass with $K_{IC} = 0.75\ \text{MPa m}^{-3/2}$, with m in Equation 13 equal to 1.3 are shown in Fig. 4b to d. Also shown are the quasi-static and dynamic stress intensity factors. The latter have been multiplied by a modifying factor so that K_{IC} for all three approaches occurs at the same time. A more detailed discussion of the crack growth resulting from these stress pulses is given in Section 5.

3. Experimental details

3.1. Specimens

Commercially available soda-lime glass blocks 15 cm x 15 cm x 2.5 cm were the main samples used in this study. Only plates relatively free of scratches and obvious damage were chosen. Prior to water-jet impact the glass plates were given an etch in a solution of ~ 10% hydrofluoric acid for approximately 2 min. This was done to blunt any pre-existing flaws in the glass surface and so prevent these flaws growing during their exposure to the stress wave. A few additional tests were carried out on similar sized blocks of a borosilicate glass and a lead glass, as well as thin discs (~ 3 mm thick) of reaction-bonded silicon nitride and a 10 mm thick plate of large grained (~ 1 cm) polycrystalline germanium. Details of all these specimens are given in Table I.

3.2. Flaw introduction

Flaws of well-defined dimensions, orientation and position were introduced onto the surface of the glass plates with a diamond Vickers pyramid. From the corners of the pyramidal impression cracks of highly reproducable dimensions were

TABLE I

Material	K_{IC}(MN m$^{-3/2}$)	V_{max}(m sec^{-1})
Germanium	0.6	
Soda-lime glass	0.75	1520
Borosilicate glass	0.8	1750
Lead glass	0.7	720
Reaction-bonded silicon nitride	2.3	2950

generated. The size of the cracks was controlled by the load on the Vickers pyramid. The mechanics of the initiation and development of these cracks has been given elsewhere [28], the cracks are very nearly semi-circular across the diagonals of the Vickers impression. It has also been noted [29] that a small component of residual stress surrounds the residual hardness impression giving rise to a residual stress intensity factor at the tips of these cracks. Cracks formed in this way were generally arranged so that one crack was parallel and one orthogonal to the incident circularly expanding stress wave front. However, a few cracks were deliberately oriented at some angle to the stress wave.

3.3. Surface-wave generation

Intense surface waves were produced by the impact of a high-velocity water jet on a glass block. The method of water-jet production was the same as that employed by Bowden and Brunton [30]. A lead slug is fired into a cylinder filled with water backed by a neoprene rubber seal, a water jet is extruded from a narrow orifice at the other end of the cylinder at much higher velocity. The velocity of the water jet is altered by changing the velocity of the lead slug with a gas gun system. The production of water jets is highly reproducible provided care is taken in filling the cylinder with water. In the present study, nozzles producing the jets were 1.6, 0.8 and 0.4 mm diameter. Most results were obtained with the 1.6 mm nozzle.

3.4. Stress-wave monitoring

The surface stress waves were monitored with a piezoelectric crystal (PZT) mounted on the surface of the glass. The PZT crystal was ~ 4 mm x 4 mm x 0.25 mm with a natural resonance frequency of ~ 10 MHz. It was imbedded in a mixture of tungsten powder and Araldite, the latter centrifuged onto the large face of the crystal, to minimize bending modes and to damp the resonance. It was then mounted with the narrow edge perpendicular to the incident wave front. A more detailed description of these transducers and their suitability for detecting surface waves has appeared recently by Harnik [34]. The output from the PZT crystal was fed directly into a storage oscilloscope. Another PZT crystal was mounted on the surface of the glass closer to the source of the stress wave and this was used to trigger the oscilloscope thus enabling the complete stress wave to be recorded. The response of the transducer and its ability to monitor Rayleigh waves was tested by dropping small steel and glass balls onto a glass block from different heights and distances.

3.5. Measurement of crack growth

Shortly after impact with the water jet, the specimen was re-etched and the size of the cracks measured. Apart from measuring the length of the longest crack, the distance to crack branching, total extension of branched cracks, angle between the branches and also the size of the ungrown branch of the initial flaw were monitored. The subsurface growth of the crack was more difficult to determine and only limited measurements were made of this aspect of crack growth.

4. Observations

4.1. Stress waves

Typical observations of the stress waves produced by a small ball impacting onto a glass block at different distances from the impact site are shown in Fig. 5. These are very similar to those predicted by Tsai and Kolsky [23] as shown in Fig. 2a. The magnitude and duration of the surface waves varied with the size of the ball, density, drop height and distance of impact from the PZT crystal. The variation of the intensity of the pulses produced by a 1.0 mm steel ball with distance from the detector are shown in Fig. 6. The slope of the line through the data is $-\frac{1}{2}$. The form of the stress pulses generated by impacting water jets are shown in Fig. 7. The stress waves observed are very similar to those generated by the steel balls in Fig. 5, only the intensity is ~ 1000 times greater and duration much shorter. By varying the trigger level and sensitivity of the oscilloscope, the arrival of the P wave could be observed. The intensity of this wave was orders of magnitude lower than the Rayleigh wave intensity. In a few cases stress drops within the near triangular pulses were observed (Fig. 7c). A similar observation has

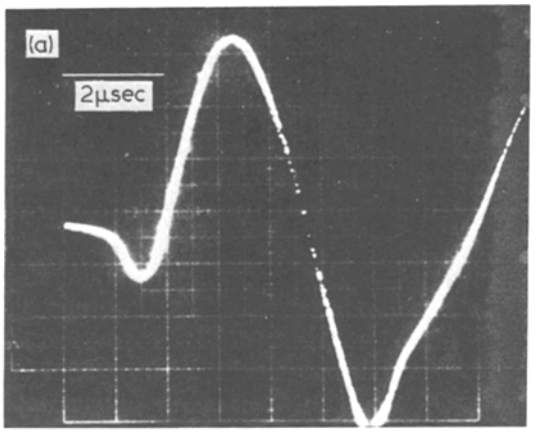

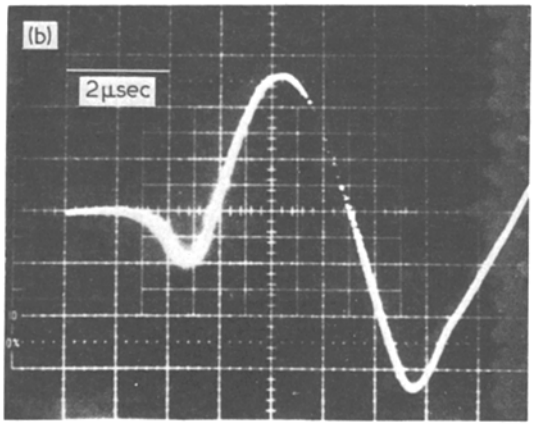

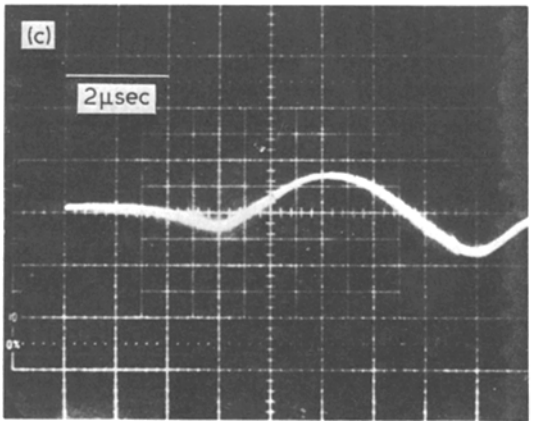

Figure 5 Surface waves produced by a 1.0 mm steel ball impacting soda-lime glass from a height of 30 cm at (a) 3 cm, (b) 5 cm and (c) 10 cm from the detector.

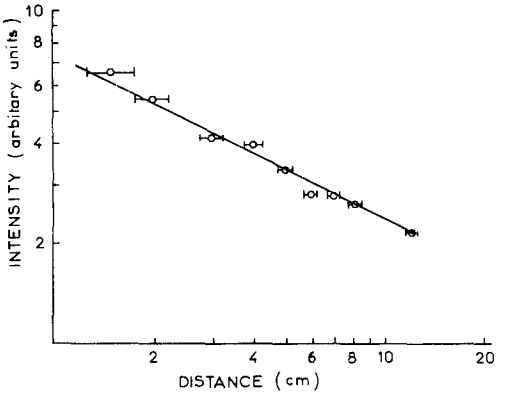

Figure 6 Variation of the intensity of the pulse produced by a 1.0 mm steel ball dropped from a height of 30 cm as a function of distance from the detector.

been reported by Tsai and Kolsky [23] and more recently by Knight *et al.* [31] when cone cracks are formed during impact loading.

4.2. Crack growth

Typical observations of the growth of the indentation flaws subjected to a Rayleigh wave produced by a 1.6 mm jet at 550 m sec^{-1} are shown in Fig. 8. In each figure, R is the radial distance from the origin of the impact and the arrow indicates the incident direction of the stress wave. The extent of branching as shown in Fig. 8 was found to be strongly dependent upon the distance from the impact site. The growth of a random flaw, not removed by the etching process, was similar to that of the introduced flaws (Fig. 9). The growth of flaws was normally straight (Fig. 8c), except when branching occurred or the initial flaw was inclined to the incident stress wave. One example of a flaw inclined at 45° to the incident stress wave is shown in Fig. 10a. In this case the extent of crack growth was slightly less than for those cracks parallel to the incident wavefront. For all inclined flaws subsequent growth was parallel to the incident wavefront. In addition, the effect of two adjacent flaws was studied; a typical observation is shown in Fig. 10b. A more detailed discussion of these latter observations has been presented elsewhere [32].

Measurements of the extent of crack growth with the 1.6 mm jet at 550 and 300 m sec^{-1} at various distances from the impact site are shown in Fig. 11.* The arrows mark the onset of crack branching at each velocity. The results are some-

* On this and subsequent figures, different symbols represent results obtained from a repetition of the test.

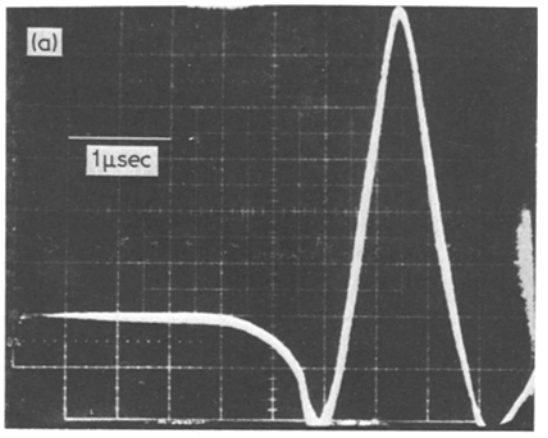

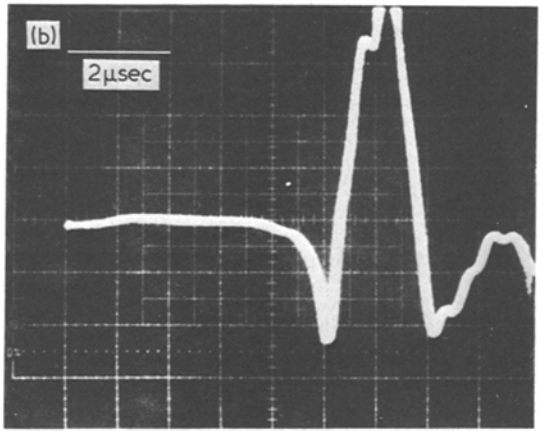

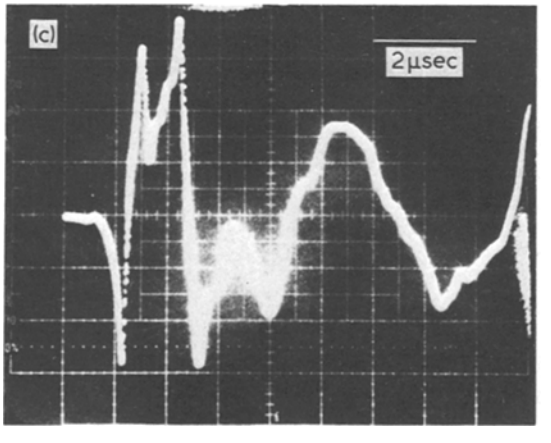

Figure 7 Surface waves produced by water jets impacting a glass block at 350 m sec^{-1} at a distance of 4.5 cm from the detector, (a) 1.6 mm jet, (b) 2.4 mm jet and (c) 2.4 mm jet.

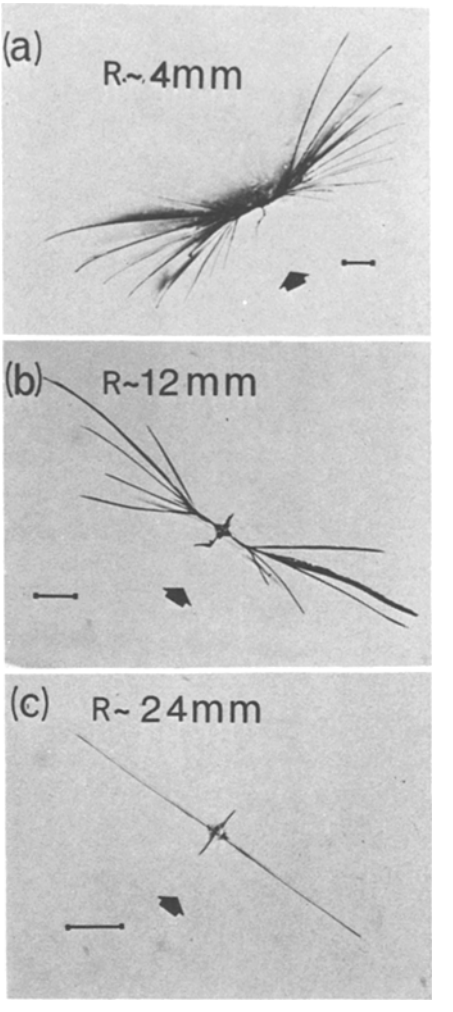

Figure 8 Observation of the surface flaws after transit of a surface wave produced by a 1.6 mm jet at 550 m sec^{-1}. The marker on each micrograph equals 100 μm.

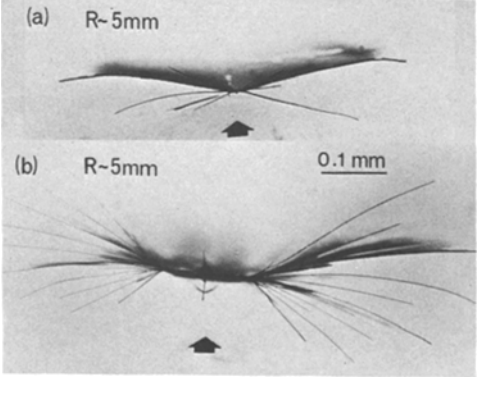

Figure 9 Comparison of the growth of a random flaw (a) not removed by etching with an introduced flaw (b), both 5 mm from the impact origin of a 1.6 mm jet at 550 m sec^{-1}.

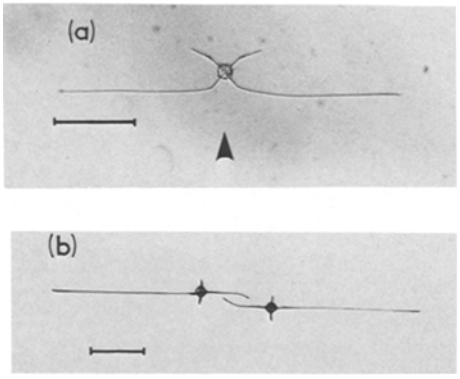

Figure 10 (a) The growth of a flaw inclined at ~ 45° to the incident surface wave. (b) The interaction of two adjacent flaws. The marker on each micrograph equals 100 μm.

what exaggerated in the vicinity of 30 mm from origin because of a reflected longitudinal wave reinforcing the surface wave intensity and increasing crack growth.

In Fig. 12 the total crack growth is plotted as a function of distance from the impact origin. For these measurements, the length of all the branches were added if the crack branched. The effect of varying the flaw size was also examined for flaws at two different distances from the

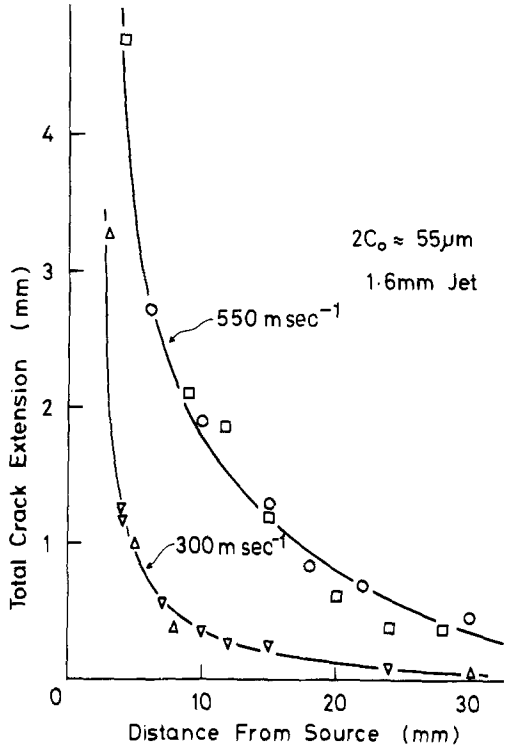

Figure 12 The total extent of crack growth for the 1.6 mm jet impacting soda-lime glass at 550 and 300 m sec^{-1}.

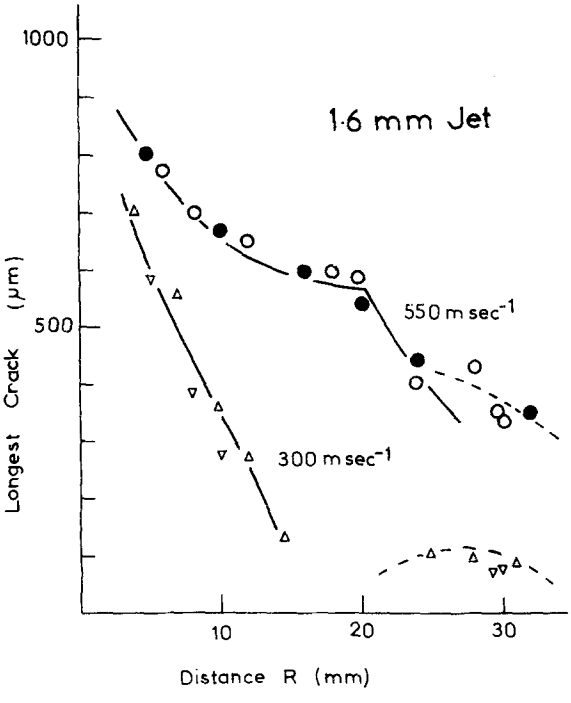

Figure 11 Growth of 55 μm flaws as a function of distance from the impact site in soda-lime glass when impacted by a 1.6 mm jet at 550 and 300 m sec^{-1}.

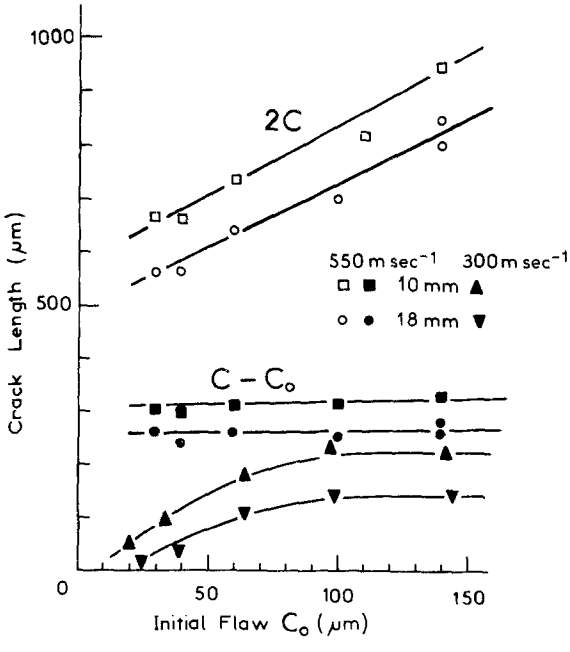

Figure 13 Crack growth as a function of initial flaw size at 10 and 18 mm from the impact site in soda-lime glass with the 1.6 mm jet at 550 and 300 m sec^{-1}.

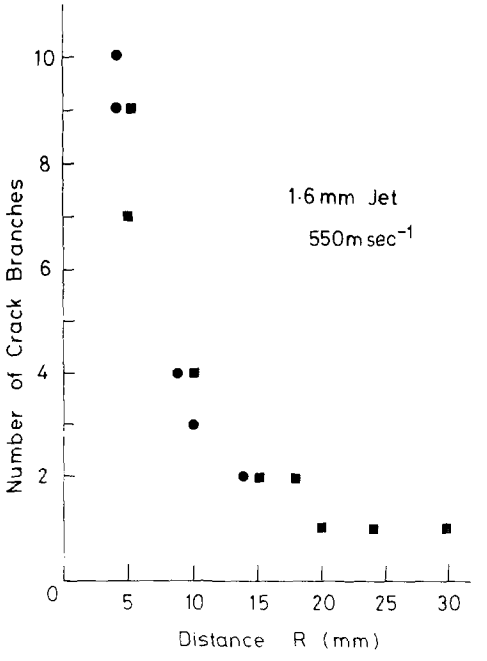

Figure 14 Number of crack branches in soda-lime glass as a function of distance with the 1.6 mm jet, at 550 m sec^{-1}.

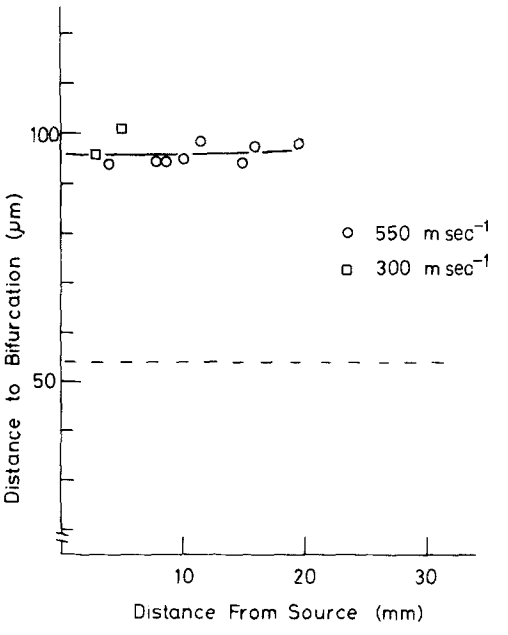

Figure 16 Distance to branching as a function of distance from the impact site in soda-lime glass when impacted with the 1.6 mm jet at 550 m sec^{-1}.

impact site with the 1.6 mm jet at 300 and 550 m sec^{-1}. It was found that the extension of the cracks was independent of the flaw size for the higher velocity jet impact, whereas at 300 m sec^{-1} there occurred a transition from flaw size dependence for small flaws to flaw size independence for larger flaws (Fig. 13). Also measured were the number of crack branches with distance from the impact site for the 1.6 mm jet at 550 m sec^{-1} (Fig. 14). The onset of crack branching occurring between 18 and 20 mm from the impact site.

The growth of the introduced cracks prior to

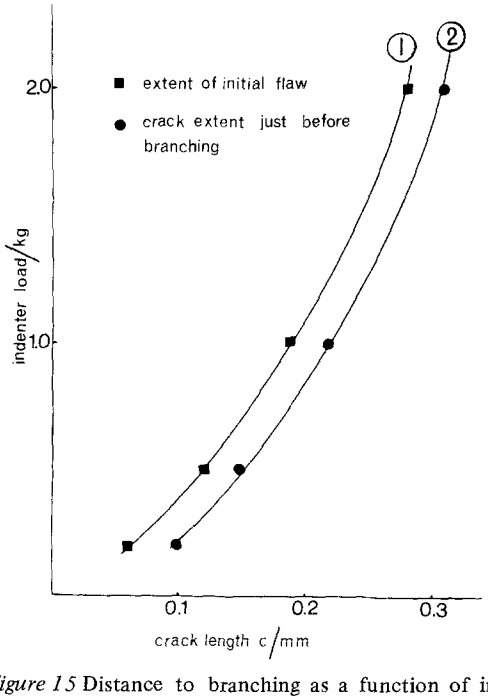

Figure 15 Distance to branching as a function of initial flaw size in soda-lime glass with 1.6 mm jet at 550 m sec^{-1}.

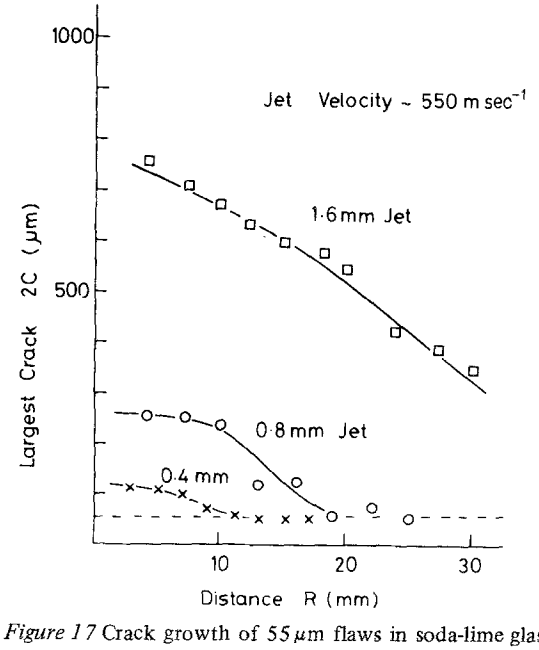

Figure 17 Crack growth of 55 μm flaws in soda-lime glass at various distances from the impact site when subjected to pulses produced by 1.6, 0.8 and 0.4 mm jets at 550 m sec^{-1}.

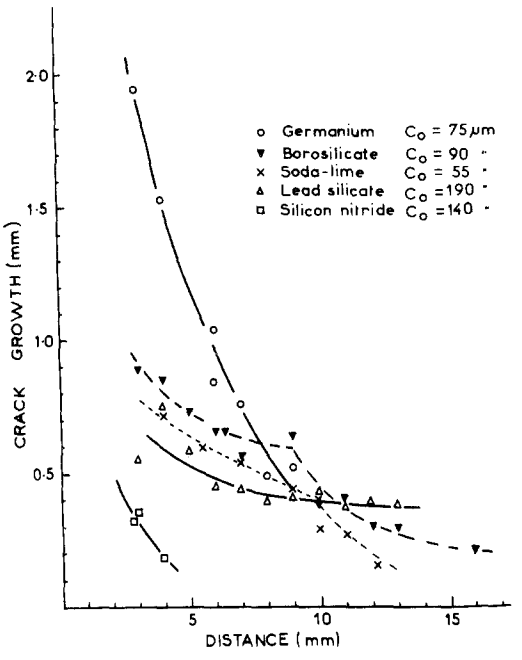

Figure 18 Comparison of the extent of crack growth of flaws in germanium, reaction-bonded silicon nitride, borosilicate, soda-lime and lead glasses when subjected to 1.6 mm jet at 300 m sec^{-1}.

branching was measured and found to be independent of the initial flaw size (Fig. 15), or distance from the impact site (Fig. 16). However, this distance is certainly greater than that of the etched and presumably rounded flaw in Fig. 9a. The growth of flaws subjected to Rayleigh waves produced by 1.6, 0.8 and 0.4 mm jets at 550 m sec^{-1} is compared in Fig. 17. Finally, the extent of crack extension produced by a 1.6 mm jet at 300 m sec^{-1} impacting a borosilicate glass, a lead glass, germanium and reaction-bonded silicon nitride, is compared with a soda-lime glass (Fig. 18).

5. Discussion

5.1. Stress-wave observations

The voltage output of PZT crystals results from changes in radial velocity of the crystal, that is, the voltage is proportional to $\partial u_r/\partial t$. However, as pointed out by Goodier *et al.* [21], if we consider the surface wave as one dimensional, than the radial strain ϵ_r is given by:

$$\epsilon_r \propto \frac{\partial u_r}{\partial r} \sim \frac{\partial u_r}{\partial t}. \qquad (14)$$

The radial stress σ_r will vary in a somewhat similar manner to ϵ_r with time. The performance of the PZT crystal will be to some extent conditioned by its frequency response. With this limitation and also the approximations made above, it is interesting to compare the observations of a trace produced by the impact of a small steel sphere (Fig. 5), with the predicted variation of radial stress by Tsai and Kolsky [23] (Fig. 2a). The agreement between the present observations and the predictions of Tsai and Kolsky is quite good, indicating that in this frequency domain the PZT crystal is responding in a linear manner. The observations in Fig. 5 and others showed no evidence of dispersion of the stress wave owing to distance travelled.

The form of the stress waves produced by the water jet are in a slightly higher frequency domain than those produced by the impacting sphere. However, the oscilloscope output is very similar to the variation of radial strain as predicted by Mooney [20] (Fig. 2b), for a finite impact loading time. The trace is considerably different from that predicted by Blowers' analysis (Fig. 3). This may be the result of the limited frequency response of the PZT crystal to the very high-frequency components in Blowers' solution or to the loss of these components owing to scattering by small surface defects. Both of these effects would "round off" the almost square waveform proposed by Blowers.

The other aspects of the present observations of the surface waves produced by ball impacts confirm the theoretical predictions. The intensity of the stress pulse with distance from the impact site (Fig. 6), is as predicted by Equation 3. Similar observations have been made by Goodier *et al.* [21]. At present, we have been unable to calibrate the PZT crystal in a satisfactory manner. However, it has been possible to infer from the threshold distance to crack extension the magnitude of the stress pulses generated by the water jets.

5.2. Crack growth

Prediction of the extent of crack growth resulting from the transit of a tensile stress wave across a flaw depends upon how well we can define the magnitude and duration of the stress pulse. The limitations of our ability to determine both these factors has already been pointed out. However, an independent estimate of the magnitude of the stress pulse may be had from the threshold distance from the impact site for the initiation of crack growth. As pointed out in Section 2, for a small crack quasi-static considerations should provide a good estimate of the critical stress necessary to initiate crack growth. The maximum

stress at the point of initiation is then:

$$\sigma_m = \frac{K}{1.3\sqrt{(\pi C)}}$$

where normally $K = K_{IC}$ but for cracks introduced by indentations $K = K_{IC} - K_R$ where $K_R \sim 0.3K_{IC}$. K_R is a residual stress intensity factor owing to the residual stress field about the permanent hardness impression [29]. On subsequent crack extension the stress intensity resulting from the permanent impression decreases as $(C_0/C)^{3/2}$.

Following the analysis presented in Section 2, the extent of crack growth for the three jet sizes studied 1.6, 0.8 and 0.4 mm has been computed. This was done by considering the duration of the surface-water pulses to be 1.0, 0.5 and 0.25 μsec, respectively, for the three jets. Crack growth as a function of the critical distance was determined for a triangular pulse and an error function-type pulse, as shown in Fig. 4a. The growth of the cracks was predicted using quasi-static, quasi-steady and an expression given by Eshelby, Equation 13. The stress pulses were subdivided into many intervals and during each interval the stress intensity factor was computed. The crack velocity was determined from the stress intensity factor using an expression given by Kerkhoff and Richter [40],

$$V = V_0(1 - K_{IC}^2/K^2),$$

where $V_0 = 1520\,\mathrm{m\,sec^{-1}}$ for soda-lime glass. This expression for crack velocity is found to fit data for soda-lime glass very well. It is very similar to the theoretical expression for crack velocity (Equation 10), except that C_r is replaced by V_0. The predictions according to the above theories with and without consideration of the indentation stresses are shown in Fig. 19a and b. The indentation stress significantly increases the threshold distance for crack extension as well as the form of the crack extension versus distance curve. The predictions for both the triangular pulse and error function pulse are in the form of upper and lower limits as determined by quasi-static and Eshelby's expression, Equation 13, respectively. Quasi-steady estimates of crack growth were found to lie between these two limits, but closer to the lower limit. The difference between the triangular and error function expressions occurs because the time for crack initiation for the latter near the threshold stress is less than for a triangular pulse.

The extent of crack growth predicted by the dynamic analysis, for the same values of maximum tensile stress, was at least five times greater than observed even with the largest crack introduced. More realistic values could be obtained if it was assumed that crack initiation only occurred if the stress intensity factor exceeded a value in excess of K_{IC}. That is, for a dynamically loaded crack $K_{ID} > K_{IC}$. Some justification for this assumption comes from the recent work of Mendiratta *et al.* [48]. These authors found that for beams of silicon nitride, pre-notched with a Knoop indenter, the critical stress intensity when dynamically loaded exceeded K_{IC}. The predictions resulting for two different values of K_{ID}, and with the condition for crack arrest as K_{IC}, are shown in Fig. 19A.

The ratio of the threshold distances may be estimated in two ways. Following Mooney [20], Equation 3, the magnitude of the Rayleigh wave is related to the duration of the pulse. That is, σ is the jet diameter r. An alternative expression, similar to a function of quasi-static Hertzian analysis is,

$$\sigma \propto \sigma_0\left(\frac{r}{R}\right)^{1/2} \propto \rho CV\left(\frac{r}{R}\right)^{1/2},$$

or the threshold distances are dependent upon, $2r$, the diameter of the contact area of the jet on the surface which is related to the diameter of the jet. That is, the ratio of the threshold distances should be 4 : 2 : 1 for the 1.6, 0.8 and 0.4 mm jets. Similarly for the same jet at two different velocities, the ratio of the threshold distances should vary as the ratio of the velocities squared. This is consistent with observations of the threshold distance for the $300\,\mathrm{m\,sec^{-1}}$ 1.6 mm jet (Fig. 11), and a similar threshold for the 0.4 mm jet at $550\,\mathrm{m\,sec^{-1}}$ (Fig. 17). The observations of the threshold distance as a function of jet diameter (Fig. 17), support the simple quasi-static approximation for the magnitude of the stress rather than the expression given by Mooney [20].

Observations of crack growth in different materials resulting from a 1.6 mm jet at $300\,\mathrm{m\,sec^{-1}}$ (Fig. 18), show a general similarity. Crack extension increases with decrease in distance from the impact site. However, upon reaching a critical distance (or stress), crack branching occurs and thereafter the extent of crack growth is almost independent of the stress. The total extent of crack growth is almost independent of the stress. The total extent of crack growth upon exceeding the threshold distance is related to the maximum crack velocity of the material. The maximum

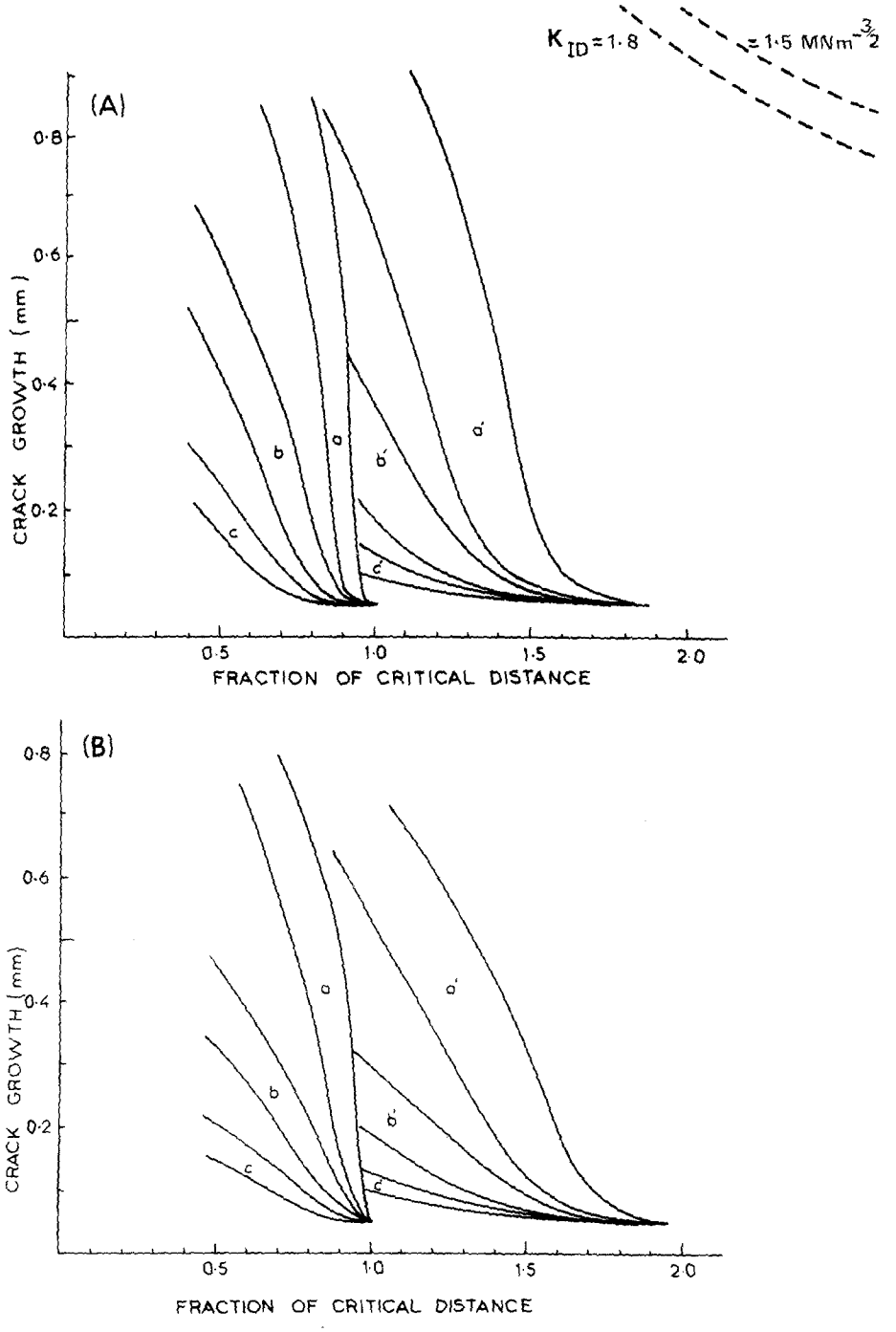

Figure 19 Predicted crack growth of 50 μm flaws as a fraction of the critical distance to crack nucleation, with and without (unprimed letters) inclusion of residual indentation stresses for the 1.6 mm jet (a), 0.8 mm jet (b) and 0.4 mm jet (c) (A) for a triangular pulse and, (B) the error function pulse. See text for details.

crack velocities for the different materials are listed in Table I. For the borosilicate and lead glasses the maximum values were determined from Schardin's [41] observations and relationship between maximum velocity, Vickers hardness and density of the glass. Branching was very occasionally observed with crack growth in germanium and cracks were found to propagate along cleavage planes even though they were slightly inclined to the stress wavefront. As mentioned above it was not found possible to predict the onset of crack branching although some idea

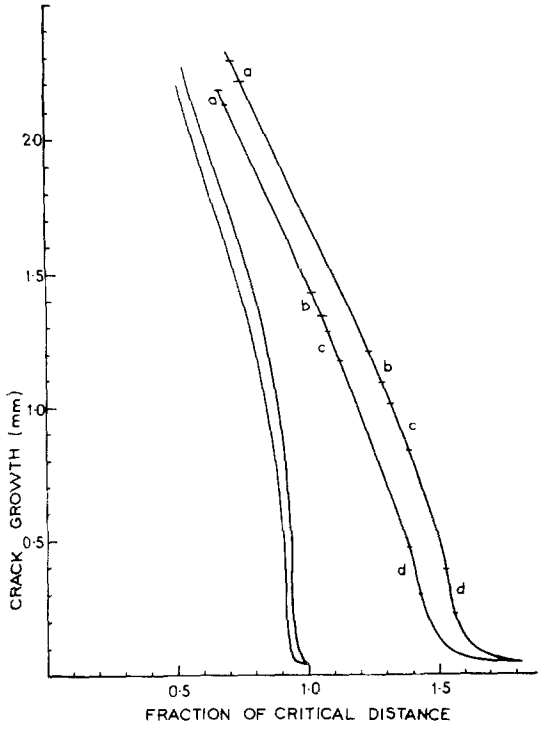

Figure 20 Prediction of crack growth for 50 μm flaws when the maximum velocity of crack propagation is the Rayleigh wave velocity, with and without indentation stress. The letters a, b, c, and d indicate the positions where the crack velocity exceeds the maximum velocity of crack propagation in germanium, borosilicate, soda-lime and lead glasses.

of the behaviour may be had by using a critical velocity criteria. If, instead of V_0 equal 1520 m sec^{-1} in the expression given by Kerkhof and Richter [40], one uses C_r for soda-lime glass, then the prediction of crack extension versus distance is shown in Fig. 20. Also marked are the positions where the crack velocity exceeds the terminal velocity of the different materials. The positions of the predicted plateau are much higher than observed which is as expected considering the criteria used together with a disregard of the expected increase of the fracture toughness with velocity prior to crack branching. However, the observations of crack growth in germanium are very similar to the predictions of Fig. 20.

The kink in the crack extension versus distance curve is no longer present at the onset of branching if one plots the total extent of crack growth against distance as shown in Fig. 11. The observation is in accord with the concept of strain energy of the body in the region of the crack in excess of an initial value being converted into new crack surface. The strain energy is proportional to σ^2 and hence to $1/R$, which is in agreement with the present observations. The observations of enhanced crack growth with the 1.6 mm jet at $\sim$ 30 mm from the origin (Fig. 11), are in agreement with previous observations by Bowden and Field [9] and have been explained in terms of reinforcement of the surface wave with reflected longitudinal and shear waves. This phenomena would be expected to become more severe with thin plates and may have the effect of lowering the threshold velocity for crack extension.

5.3. Crack branching

Previous investigations of the bifurcation of rapidly propagating cracks in brittle materials have usually considered tensile loading of beams or plates. Under these conditions, the initial crack grows some 10 to 50 times its own length before the onset of branching. When branching does occur it is usually into only two branches which often branch on further growth. Typically the half angle between the two branches is $\sim 20°$, in agreement with a recent theoretical treatment by Bilby *et al.* [35]. The present observations (Fig. 8) support this conclusion when only two branches are formed; but upon multiple branching the half angle between the branches is usually smaller.

A number of criteria have been proposed for the onset of crack branching. Yoffe [36] found that for a crack propagating at a velocity greater than half the Rayleigh wave velocity, the maximum tensile stress was no longer directly ahead of the crack tip. Some support for this mechanism of crack branching has recently come from observations of cleavage controlled crack growth in quartz [37]. However, for glasses, crack branching is observed to occur at or below $C_r/2$. An alternative proposal by Rose [43] is that crack branching will occur if the fracture toughness increases with crack velocity. This concept is not considerably different from proposals put forward by Eshelby [38] and more recently Döll [39]. Eshelby proposed that if the energy absorbed by the moving crack was twice the quasi-static energy for crack formation, G_{IC}, then branching would occur with a considerable reduction in crack speed. That is

$$G_b \geqslant 2G_{IC} \quad \text{or} \quad G_{nb} \geqslant nG_{IC}$$

where n is the number of crack branches. Döll [39] has modified this criteria in the light of experimental evidence to the condition that the

absorbed energy exceeds twice the energy to reach the maximum crack velocity, that is

$$G_b \geqslant 2G_{V_{max}} \quad \text{or} \quad G_{nb} \geqslant nG_{V_{max}}.$$

Using this approach, with a quasi-static estimate of G_b, it is possible to predict the number of branches that should be formed as a function of distance from the impact site. The quasi-static energy absorbed by a crack at branching is

$$G_{nb} \propto \frac{\sigma^2 C_b}{E},$$

where C_b is the crack length at branching and σ is the maximum tensile stress. As shown in Fig. 16, C_b was found to be independent of the number of crack branches, and for a Rayleigh wave the stress is proportional to $R^{-1/2}$. Therefore, the above expression reduces to

$$G_{nb} \geqslant nG_{V_{max}} \propto 1/R.$$

That is, the number of crack branches varies inversely with the distance from the source. For the 550 m sec^{-1} jet the onset of crack branching occurred at 20 mm from the impact site. It is now possible to predict the number of crack branches as a function of distance.

Good agreement is found between predicted and observed number of crack branches as shown in Fig. 14.

The present observations that the distance to crack branching is independent of stress are markedly different from typical observations of crack branching resulting from quasi-static loading of cracks [44]. Under these conditions the typical growth of the initial crack to branching is approximately 9 times, the typical mean acceleration rate being $\sim 4 \times 10^7$ m sec^{-2}. In the present observations, the growth to crack branching is less than the original flaw size and is found to be independent of the stress and initial flaw size. The typical mean acceleration rate for these cracks is $\sim 3 \times 10^{10}$ m sec^{-2}.

The observations may indicate that the acceleration rate is too rapid and this may be an additional limitation to the extent of crack growth. Glennie and Willis [45] have predicted such behaviour for a crack propagating in materials with a Dugdale type plastic zone at the crack tip.

Alternatively, these observations may be interpreted in terms of the stress intensity factor at crack initiation being much greater than K_{IC}. A similar phenomena occurs for specimens with a blunt notch wherein the crack initiates with a finite velocity [37, 38].

5.4. Residual strength

The residual strength of brittle solids impacted with water jets may be determined from the analysis presented here. In Figs. 19 and 20, crack growth is plotted as a function of critical distance R_c/R from the impact site. For the case of 50 μm flaws the residual strength/initial strength is proportional to $(C_0/C)^{1/2}$. Again the predictions using a quasi-static approach and Equation 13 provide upper and lower bounds for the prediction of residual strength of impacted bodies. The quasi-static predictions as shown above gave a slightly overestimated value and hence might be expected to provide a conservative basis for evaluating the residual strength. Residual strength as a function of normalized velocity is plotted in Fig. 21 for the 1.6, 0.8 and 0.4 mm jets. These plots were determined from the data generated for a 50 μm flaw but similar behaviour might be expected for different initial flaw sizes. The predicted rapid fall off in strength above the threshold velocity, particularly for the 1.6 mm jet, is in good agreement with observation by Field *et al.* [42] of residual strength of impacted glass discs. The broken lines in Fig. 21 is meant to indicate the onset of branching and its effect on the expected residual strength data. Above this velocity the longest crack introduced by the water jet is very insensitive to jet velocity.

6. Conclusions

The present study has been primarily concerned with the growth of surface flaws when subjected to very short duration Rayleigh waves. The form

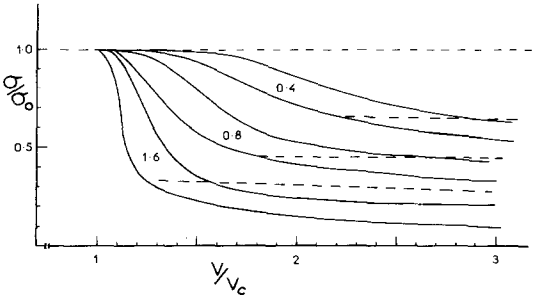

Figure 21 Prediction of the residual strength of impacted glass plates subjected to 1.6, 0.8 and 0.4 mm jets. The residual strength is plotted as a fraction of its original value and the velocity is normalized to the threshold velocity.

of the stress waves generated by the impacting water jet was monitored using a piezoelectric crystal and found to be closer in form to that predicted by Mooney [20] than that predicted by Blowers analysis [14]. The extent of growth of artificially introduced flaws was studied using three different water jet diameters. It was found that the observed growth of these flaws was similar to that of random surface flaws. The extent of growth was predicted using dynamic, quasi-steady and quasi-static estimated values of the stress intensity factor. The quasi-static approach was found to provide the most reasonable estimates when allowance was made for residual indentation stresses. Cracks subjected to stresses in excess of a critical value were found to branch but unlike previous quasi-static observations the growth prior to crack branching was found to be independent of stress or flaw size. This observation may agree with a theoretical treatment of the growth of cracks by Glennie and Willis [45] in which the acceleration rate is limited by a small plastic zone ahead of the crack tip. Crack branching in conjunction with maximum crack velocity was found to provide the limiting conditions for the extent of crack growth beyond the onset of branching. Finally, the residual strength of impacted materials as a function of velocity in excess of a threshold velocity is predicted.

Whilst it was found that the quasi-static approach could be used to give an upper estimate of the crack growth, and hence a conservative basis for residual strength determinations, it was far from satisfactory in accounting for all the observations. In particular, the observation of the independence of the crack growth on the initial flaw size, above a certain stress level or flaw size, is a basic contradiction to a quasi-static approach.

The dynamic fracture mechanics analysis tended to predict crack extensions much in excess of the observations. More realistic predictions could be obtained by assuming the stress intensity factor for crack initiation was significantly in excess of K_{IC}.

Acknowledgements

This work was supported by the Ministry of Defence (Procurement Executive). The authors thank L. Bond for advice in the fabrication of the PZT crystals used and for informative discussions, together with J. D. Eshelby, J. E. Field and B. R. Lawn. One of us, MVS, is grateful to St Gobain for financial support during the latter part of this work.

References

1. G. C. SIH, G. T. EMBLY and R. J. RAVERA, *Int. J. Solids and Struct.* 8 (1972) 977.
2. S. A. THAU and T. H. LU, *ibid* 7 (1971) 131.
3. L. B. FREUND, *J. Mech. Phys. Solids* **20** (1972) 129, 141; **21** (1973) 47; **22** (1974) 137.
4. J. F. KALTHOFF and D. A. SHOCKEY, *J. Appl. Phys.* **48** (1977) 986.
5. O. VARDAR and I. FINNIE, *Int. J. Fracture* **13** (1977) 115.
6. L. B. FREUND, "Development in Mechanics", Vol. 6, Proceedings of the 12th Midwestern Mechanics Conference (1970) p. 489.
7. H. W. REINHARDT and J. W. DALLY, *Materials Eval.* (1970) 213.
8. L. BOND, *Ultrasonics* **17** (1979) 71.
9. F. P. BOWDEN and J. E. FIELD, *Proc. Roy. Soc.* **A282** (1964) 331.
10. J. E. FIELD, *Phil. Trans. Roy. Soc.* **A260** (1966) 86.
11. D. G. RICKERBY, Ph.D thesis University of Cambridge (1977).
12. A. G. EVANS, *J. Amer. Ceram. Soc.* **56** (1973) 405.
13. W. ADLER, *J. Mater. Sci.* **12** (1977) 1253.
14. R. M. BLOWERS, *J. Inst. Math. Applics* **5** (1969) 167.
15. A. G. EVANS and T. R. WILSHAW, *J. Mater. Sci.* **12** (1977) 97.
16. H. LAMB, *Phil. Trans. Roy. Soc.* **A203** (1904) 1.
17. C. L. PECKERIS, *Proc. Nat. Acad. Sci.* **41** (1955) 469.
18. G. MILLER and H. PURSEY, *Proc. Roy. Soc.* **A223** (1954) 521; **A233** (1955) 55.
19. H. M. MOONEY, *Bull. Seis. Soc. Amer.* **64** (1974) 473.
20. *Idem, Geophysics* **41** (1976) 243.
21. J. N. GOODIER, W. E. JAHSMAN and E. A. RIPPERGER, *J. Appl. Mech.* **26** (1959) 3.
22. F. R. BRECKENRIDGE, C. E. TOCHIEGG and M. GREENSPAN, *J. Acoust. Soc. Amer.* **57** (1975) 626.
23. Y. M. TSAI and H. KOLSKY, *J. Mech. Phys. Solids* **15** (1967) 263; **16** (1968) 133.
24. J. D. ACHENBACH and R. NEIUSMER, *Int. J. Fract. Mech.* 7 (1971) 77.
25. K. B. BROBERG, *Ark. Fiz.* **18** (1960) 159.
26. A. G. EVANS, in "Fracture Mechanics of Ceramics", Vol. 3, edited by R. C. Bradt, D. P. H. Hasselman and F. F. Lange (Plenum Press, New York, 1978) p. 303.
27. K. F. GRAFF, "Wave Motion in Elastic Solids" (Clarendon Press, Oxford, 1975) Ch. 6.
28. B. R. LAWN and M. V. SWAIN, *J. Mater. Sci.* **10** (1975) 113.
29. M. V. SWAIN, *ibid* **11** (1976) 2345.
30. F. P. BOWDEN and J. H. BRUNTON, *Proc. Roy. Soc.* **A263** (1961) 433.
31. C. G. KNIGHT, M. V. SWAIN and M. M. CHAUDHRI, *J. Mater. Sci.* **12** (1977) 1573.
32. M. V. SWAIN and J. T. HAGAN, *Eng. Fract. Mech.* **10** (1978) 299.

33. H. BERGKVIST, *J. Mech. Phys. Solids* **21** (1973) 229.
34. E. HARNIK, *J. Phys. E. Sci. Instrum.* **10** (1977) 1217.
35. B. A. BILBY, G. E. CARDEW and I. C. HOWARD, Proceedings of the 4th International Fracture Conference, Waterloo, Canada, June (1977).
36. E. H. YOFFE, *Phil. Mag.* **12** (1951) 739.
37. A. BALL and B. W. PAYNE, Proceedings of the 4th International Fracture Conference, Waterloo, Canada, June (1977).
38. J. D. ESHELBY, in "Inelastic Behaviour of Solids", edited by M. F. Kanninen (McGraw Hill, New York, 1970).
39. W. DÖLL, *Int. J. Fract. Mech.* **33** (1975) 184.
40. F. KERKHOFF and H. RICHTER, Proceedings of the 2nd International Conference of Fracture, Brighton, paper 40 (1969).
41. H. SCHARDIN, in "Fracture", edited by B. L. Averbach, D. K. Felbeck, G. T. Hahn and D. A. Thomas (Wiley, New York, 1959).
42. J. E. FIELD, J. J. CAMUS, D. A. GORHAM and D. G. RICKERBY, Proceedings of the 4th International Conference on Rain Erosion and Allied Phenomena, Meersberg, May (1974).
43. L. R. F. ROSE, *Int. J. Fract. Mech.* **12** (1976) 799.
44. J. T. HAGAN, M. V. SWAIN and J. E. FIELD, *Phil. Mag.*
45. E. B. GLENNIE and J. R. WILLIS, *J. Mech. Phys. Solids* **19** (1971) 11.
46. W. JOHNSON and G. W. VICKERS, *J. Mech. Eng. Sci.* **15** (1973) 302.
47. J. E. FIELD and M. B. LESSER, *Proc. Roy. Soc.* **A357** (1977) 143.
48. M. G. MENDIRATTA, J. WIMMER and I. BRANSKY, *J. Mater. Sci.* **12** (1977) 212.

Received 13 June and accepted 2 July 1979.